



Performance assessment of railway multispan steel truss bridge bearing by thermal excitation

Naijie Han¹ · Weigang Zhao^{2,3} · Bo Zhang⁴ · Hao Zhang^{3,5} · Liming Zhou³

Received: 21 June 2021 / Revised: 15 August 2021 / Accepted: 11 October 2021 / Published online: 7 November 2021
© Springer-Verlag GmbH Germany, part of Springer Nature 2021

Abstract

The performance of bridge expansion devices (e.g., bearings or expansion joints) is a major concern for the operation department. A mechanical analysis model can be used to accurately analyze the influence mechanism of major factors and evaluate the working performance of bridge expansion devices with structural health monitoring data. Considering the nonlinear characteristics of bearing friction, a friction hysteresis model was established in this study to analyze the behavior of the bearing longitudinal displacement (BLD) under thermal excitation. The friction hysteresis model can describe the motion path of the BLD under periodic temperature. The variation in the model parameter is defined as an evaluation index that can reflect the degradation in the working performance of the bearing. The periodic change in the temperature is the driving force for developing the friction hysteresis model, and the calculation of the temperature-induced BLD is critical in extracting the evaluation index. Therefore, a calculation formula for the BLD of the steel truss bearing was derived considering the temperature gradient. Finally, the application of this method was verified through the temperature and BLD monitoring data of a multispan continuous steel truss arch bridge. The results showed that the evaluation index variance can describe the maximum bearing friction increase. However, the proposed approach is primarily based on thermal excitation, because of which it cannot assess the bearing working performance if the uncertainty in the friction hysteresis model is introduced by other types of excitations (e.g., vehicle excitation).

Keywords Steel truss bridge · Temperature gradient · Bearing friction · Bearing longitudinal displacement · Bearing working performance

1 Introduction

To ensure that bridges adapt to longitudinal deformation, expansion devices, such as rolling bearings and expansion joints, are installed at appropriate positions on the bridge. Research is being conducted on premature failures of expansion devices due to uninterrupted wear, such as periodic temperature loading and repetitive impact of vehicle loads [1–3]. For example, the expansion joints of the Runyang Suspension Bridge with a main span of 1490 m had to be repaired only after three years in service [3]. The Akashi-Kaikyo Suspension Bridge with a main span of 1991 m exhibited fatigue cracks in the connection pin of the expansion joints only three years after its opening [4]. The Jiangyin Suspension Bridge with a main span of 1385 m suffered excessive wear and transversal shear failure of the bearings in the expansion joints after only four years of operation [5]. Therefore, the maintenance of expansion devices has been a concern for bridge management.

✉ Weigang Zhao
zhaowg@stdu.edu.cn

¹ School of Civil Engineering, Shijiazhuang Tie Dao University, Shijiazhuang 050043, China

² The Key Laboratory for Health Monitoring and Control of Large Structures of Hebei Province, Shijiazhuang 050043, China

³ Structure Health Monitoring and Control Institute of HeBei Province, Shijiazhuang 050043, China

⁴ School of Civil Engineering, Beijing Jiaotong University, Beijing 100044, China

⁵ State Key Laboratory of Mechanical Behavior and System Safety of Traffic Engineering Structures, Shijiazhuang Tiedao University, Shijiazhuang 050043, China

The results of thermal-induced testing are susceptible to changes in geometric or material properties of structural systems that have been explicitly used as damage indicators [6, 7]. Damage is defined as unintentional changes to physical properties, such as boundary conditions and structural continuity, that affect structural behavior [8]. Structural health monitoring (SHM) has been widely used in bridge assessment [9, 10]. The temperature–displacement relationship model has been used to assess the working performance of bridge expansion joints or bearing based on SHM. For example, using SHM monitoring data, Ni et al. [11] estimated the maximum displacement range and cumulative movement by linear regression of the effective temperature and longitudinal displacement, and evaluated the working performance of expansion joints by cumulative movement. Deng et al. [12] pointed out that the longitudinal displacement of a suspension bridge is strongly correlated to the temperature, and a linear regression model of the average temperature was established to predict the longitudinal displacement. However, a linear regression model has drawbacks because of the uncertainty in using the effective or average temperature to simplify the temperature gradient. As a result, combining the Bayesian regression model with reliability theory, Ni [13] developed an anomaly index to evaluate the health of expansion joints and raise an alarm in the event of damage. Huang [14] introduced correlation analysis algorithms into the displacement–temperature relationship and proposed a method of early alarm to evaluate the performance of expansion joints. Given the influence of the temperature gradient, Wang [15] proposed a displacement–temperature linear regression model to predict the bearing longitudinal displacement (BLD). To alleviate the effect of the temperature gradient, Yarnold [16] selected a time window with a lower solar radiation level to describe the nonlinear mechanism of the temperature and longitudinal strain. Winkler [17] formulated the relationship between the temperature and the displacement of bridge expansion joints and used it to assess the performance of expansion joints.

Besides, The influence of boundary conditions on the BLD is significant. Yarnold [18] introduced a longitudinal nonlinear spring to study the nonlinear stick–slip displacement mechanism during the measurement period. Murphy [19] used boundary condition parameters to represent the current state of the Route 61 Bridge based on the temperature-based structural identification scheme. Xia [20] theoretically derived the linear longitudinal boundary stiffness identification method for a long-span suspension bridge based on temperature-induced effects.

A friction-based bearing system is a common expansion device for bridges. However, it is currently difficult to express the BLD in mathematical formulae under the

bearing friction and nonuniform temperature fields, which limits the interpretability of evaluation methods based on thermal excitation. Finite element model modification techniques have been applied to determine the longitudinal boundary stiffness in many studies [6, 21–23]. Satisfactory results could only be obtained when repeatedly adjusting the finite element model parameters; this requires a considerable amount of work if the finite element model is complex. To solve the above problems, in this study, a frictional hysteresis model was established to analyze the BLD behavior under bearing friction and nonuniform temperature fields, and a temperature-induced BLD computational formula was derived considering the temperature gradient. A method for assessing the bearing working performance was developed based on monitoring data.

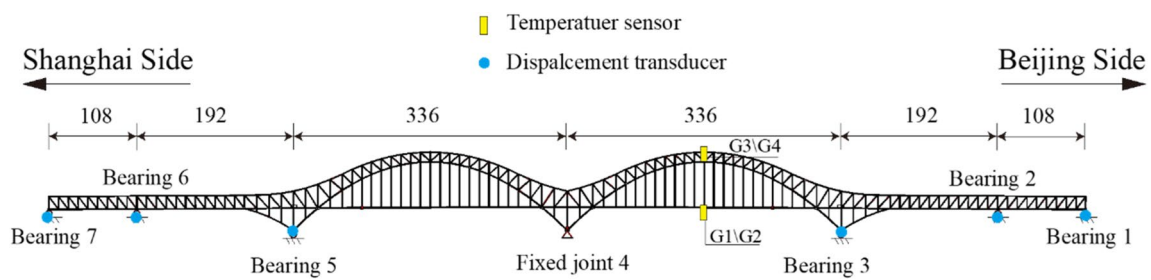
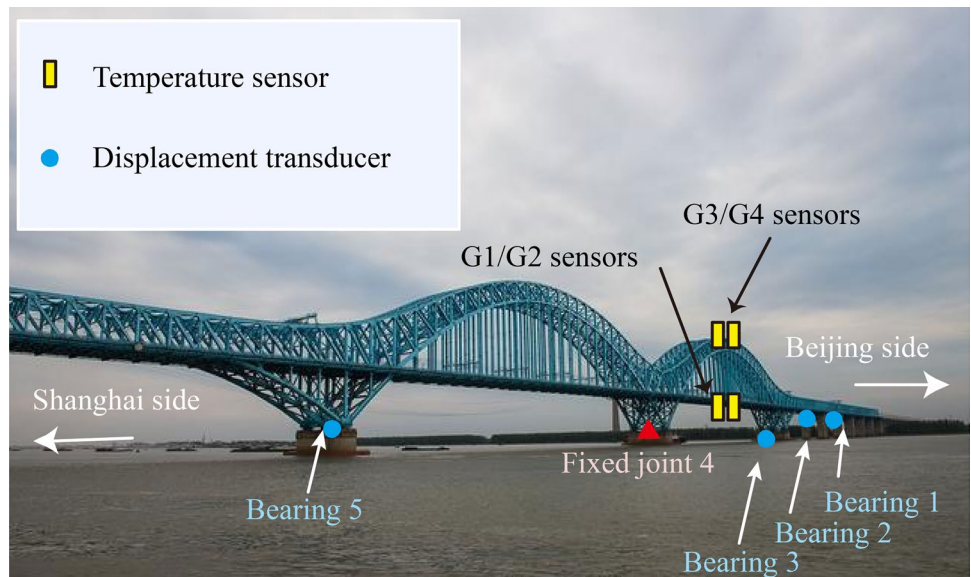
2 Characteristics of truss bridge BLD under operational condition

A railway multispan continuous steel truss arch bridge is a symmetric structure with a main span of 336 m and spans of 108 and 192 m on either side (Fig. 1). The truss bridge is composed of a steel truss frame and a steel deck. Spherical bearings are installed on the bridge to release the longitudinal displacement, whose sliding material is polytetrafluoroethylene. Displacement transducers are installed at all the bearing positions except at the fixed joint 4. The positive direction of the BLD is defined as the deviation in the bearing from the initial position toward Beijing. Four Fiber Bragg grating temperature sensors are installed on the cross sections of the upper and lower chords, as shown in Fig. 2b.

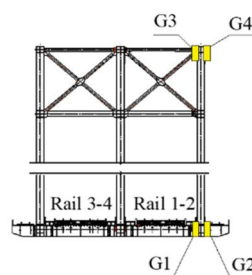
Figure 3 shows 480 h of BLD monitoring data. The curve trend of BLD 1–BLD 3 (longitudinal displacement monitoring data of bearings 1–3) is consistent; however, the curve of BLD 3 is evidently rough. Figure 4 shows 24 h of BLD monitoring data. The train-induced BLD was marked based on the train passing signal collected by the monitoring system. It indicates that the train has a negligible effect on BLD 1 and BLD 2; BLD 2 has a dead zone in the region of extreme point of temperature (i.e., when the temperature changes, BLD 2 remains stationary). “Dead zone” was defined as “stick” in literature [24], as shown in Fig. 5, indicating that the bearing friction has a non-negligible influence on the BLD. Accordingly, a BLD analysis model under temperature and bearing friction is proposed in Sect. 3.

Figure 6 shows the influence of trains on BLD 3: after the train runs over the bridge, not all BLD 3 can return to its initial state. This indicates that the bearing friction may change when trains pass. The reasons will be discussed in the last section.

Fig. 1 The continuous truss bridge site



(a) Sensors installation and truss bridge elevation



(b) Temperature sensors cross-section

Fig. 2 Layout of sensors on the continuous truss bridge(unit:m): **a** sensors installation and truss bridge elevation; **b** temperature sensors cross section

3 Friction hysteresis model and evaluation index

3.1 Analysis for simply supported beam

Figure 7 shows the friction-based bearing systems for a simply supported beam. The meanings of each element name are as follows:

Nomenclature for Fig. 7

Thermal expansion element (TEE): with infinite axial stiffness to simulate the thermal expansion characteristics of the girder.

L : The original length of the beam.

ΔT : Temperature variation of the beam.

y : BLD.

f : The bearing friction.

y_0 : Temperature-induced BLD.

M : The mass of the girder assigned to the bearing.

K : Axial stiffness of spring.

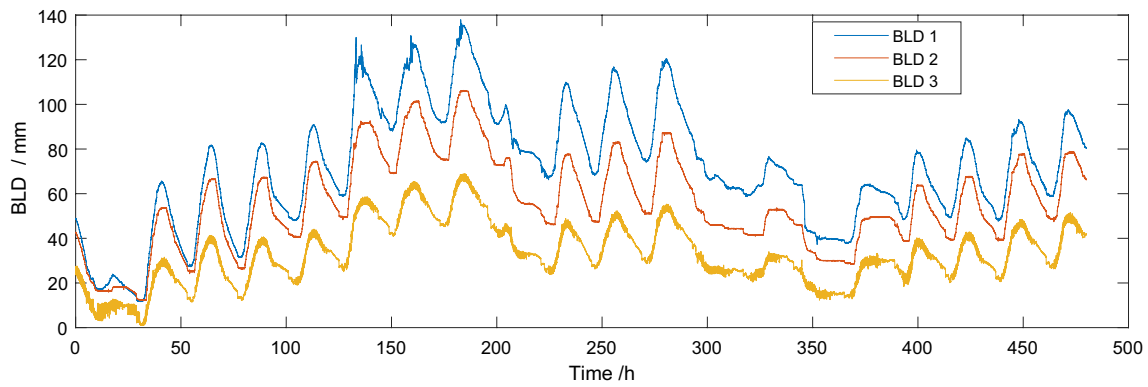


Fig. 3 BLD 1–3 time history in 480 h

Fig. 4 BLD 1–3 and temperature in 24 h

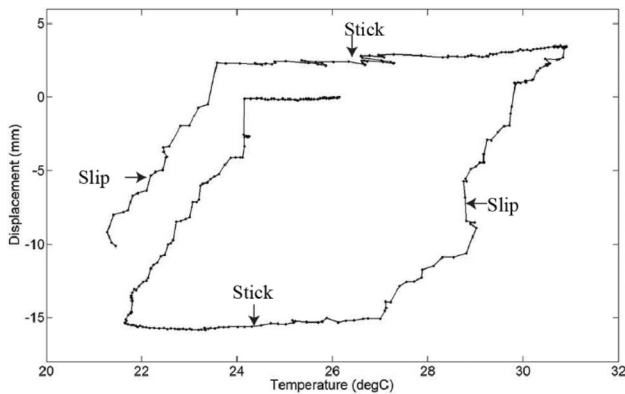
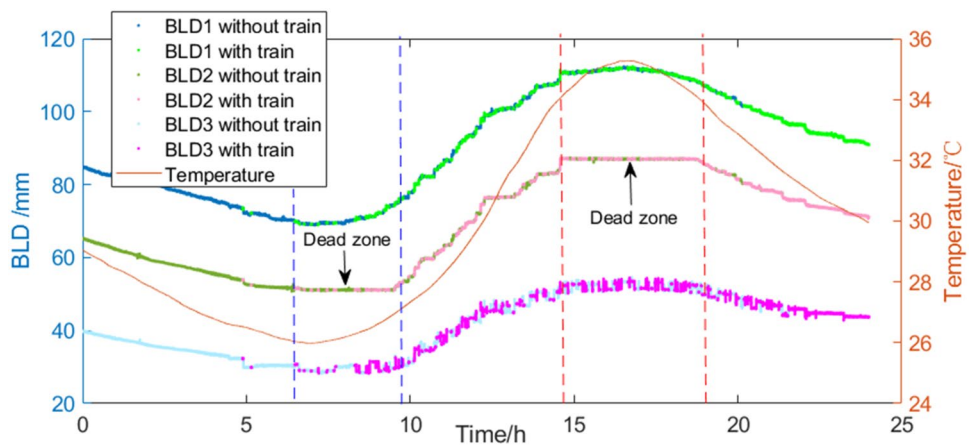


Fig. 5 Bearings displacement “stick–slip” behavior under periodic temperature

L_f : Friction-induced BLD.

C : Maximum friction-induced BLD.

Bridge materials, such as steel and concrete, expand and contract in response to thermal “loads.” A critical aspect of the thermal behavior is that the response is a combination of an unrestrained portion and a restrained portion [16]. In this friction-based bearing system, the BLD (y) is made up

of temperature-induced BLD (y_0) and friction-induced BLD (L_f). Their relationship can be expressed as Eq. (1):

$$\begin{cases} y = y_0 + L_f \\ y_0 = \alpha \Delta T L \\ L_f = f / K \\ C = \mu M g / K \end{cases}, \quad (1)$$

where α is the expansion coefficient, and μ is the frictional coefficient.

Essentially, the bearings do not move until the maximum static friction is overcome. When a bearing is restrained by the static friction, with the deformation of the spring (L_f) neutralizing the thermal deformation of the TEE (y_0), the bearing is in the “stick” position. After the generated spring force overcomes the maximum static friction ($\mu M g$), “slip” occurs as the TEE expands or contracts. Therefore, in the morning when the structure begins to heat up, the bearing is in the “stick” position until a temperature is reached, which exerts a sufficient longitudinal force. The bearing then “slips” and continues to move until the structure starts to cool. An ideal analysis model is

accordingly proposed. The friction as the boundary condition existing on the bearing restrains the BLD. The positive bearing friction (PBF) and negative bearing friction

(NBF) convert to each other when the beam is subjected to a periodic temperature load (Fig. 8a).

Process 1: 0–1. When the temperature increase, TEE expands. Since the internal force of the spring is less than

Fig. 6 The impact of trains passing on BDL 3

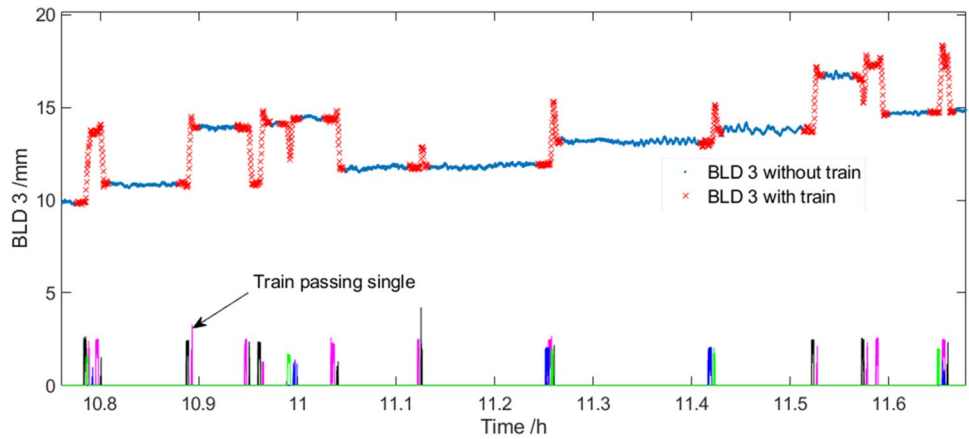


Fig. 7 The model of BLD on the effect of temperature and friction: **a** the calculation illustration of BLD; **b** the components of BLD; **c** the nonlinear of friction

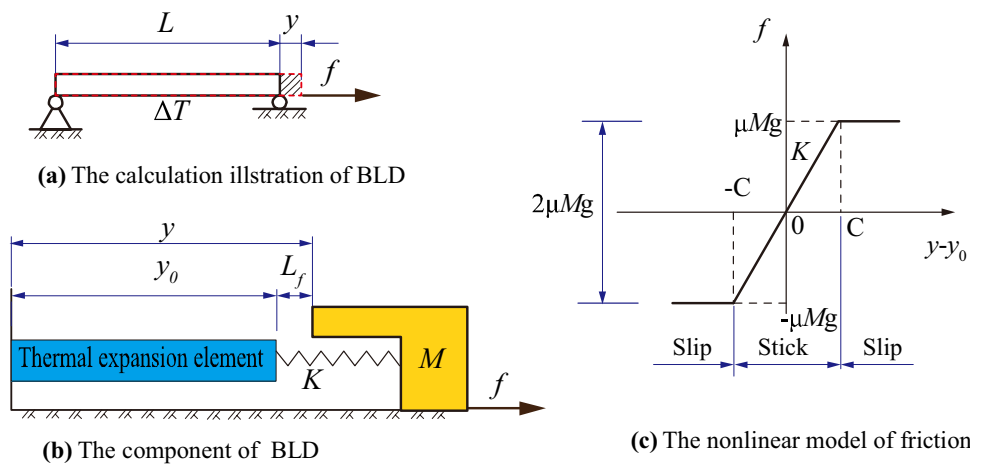
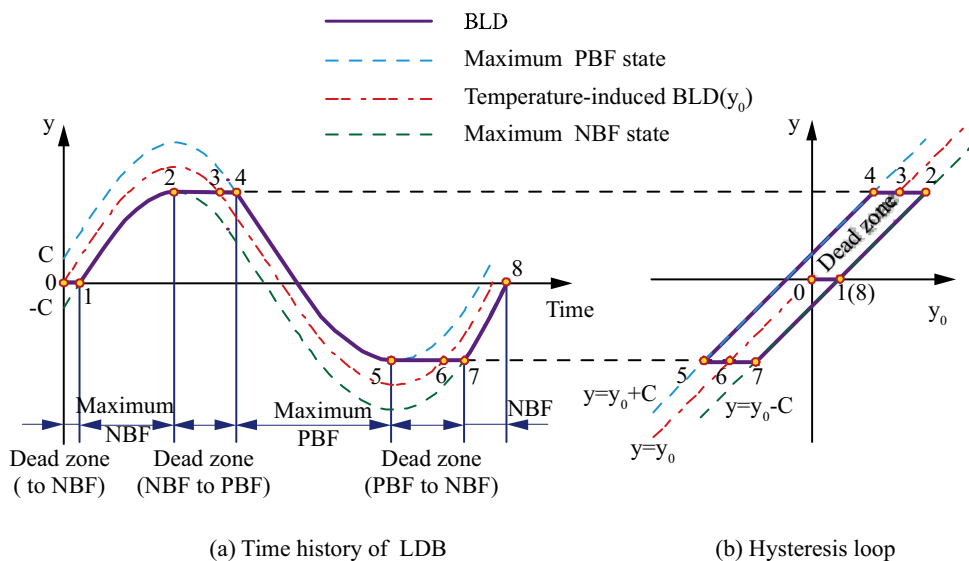


Fig. 8 The motion path of BLD and friction hysteresis model: **a** time history of BLD; **b** hysteresis loop



the maximum bearing friction (μMg), BLD does not increase immediately, and NBF occurs simultaneously.

Process 2: 1–2. When the spring internal force is accumulated by the maximum friction force (μMg), the BLD moves with TEE expansion. The NBF and the deformation of the spring remain constant.

Process 3: 2–3. When the maximum temperature is reached, the temperature begins to drop, prompting the TEE to shrink. Since the spring gradually returns to its original length from the compressed state at this time, the friction decreases to 0, and BLD remains stationary.

Process 4: 3–4. The spring turns into tension, and the friction is reversed, leading to PBF.

Process 5: 4–5. When the internal force of the spring under tension increases to the maximum bearing friction (μMg) and the temperature continues to decrease, the BLD also decreases. The deformation of the spring remains constant at this time until it drops to the minimum point.

Process 6: 5–6. The temperature begins to rise, the TEE begins to expand, the spring returns to its original length from the tensioned state, and the friction force decreases to zero.

Process 7: 6–7. Repeat process 1.

Process 8: 7–8. Repeat process 2.

The hysteresis loop (Fig. 8b) can describe the relationship between the BLD and temperature-induced LBD, such as the cyclic bilinear behavior and hysteresis characteristics. The hysteresis loop can be expressed as Eq. (2):

$$\begin{cases} y = y_0 - \frac{\mu Mg}{K} \cdot \text{sign}(y_0 - y), & |y - y_0| \geq \frac{\mu Mg}{K} \\ \dot{y} = 0, & |y - y_0| < \frac{\mu Mg}{K} \end{cases} \quad (2)$$

Assuming K is a constant, we have:

$$\Delta L_f = 2C = 2K^{-1} \mu Mg. \quad (3)$$

The hysteresis loop can be described using the parameter ΔL_f , which is proportional to the bearing friction (μMg). The parameter ΔL_f increases as the working performance of the bearing deteriorates. The relationship between ΔL_f and the maximum bearing friction for a simply supported beam is clear. However, it will be more complicated when a multispan continuous beam is introduced.

3.2 Analysis for multispan continuous beam

Typically, the displacement transducers is installed at the junction of the pier and beam. Therefore, the BLD reflects the change in the length of the lower surface of the beam instead of the change in the length of the neutral axis. For example, the friction-induced BLD for a three-span continuous beam (Fig. 9) is analyzed and calculated. The bearing friction acts on the continuous beam in the longitudinal

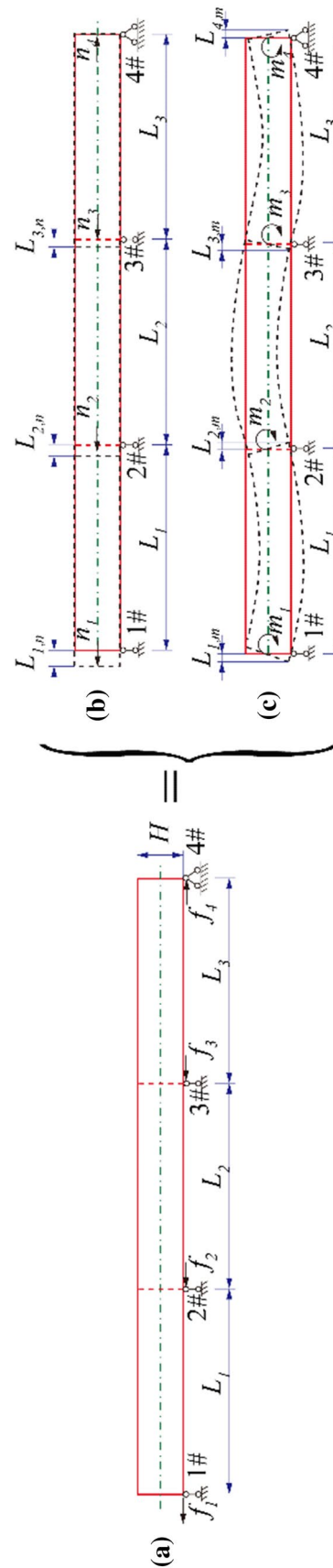


Fig. 9 The calculation illustration for friction-induced BLD, a bearing friction load on the continuous beam, b axial induced BLD, c bending induced BLD

direction as an eccentric load (Fig. 9a) and induces axial deformation (Fig. 9b) and bending deformation (Fig. 9c). Evidently, the bending deformation can induce BLD. Based on the linear elasticity theory, the friction-induced BLD is composed of two parts, shown in Fig. 9.

The friction-induced BLD can be written as a vector:

$$L_f = L_n + L_m, \tag{4}$$

$$L_f = \begin{Bmatrix} L_{f,1} \\ L_{f,2} \\ L_{f,3} \\ L_{f,4} \end{Bmatrix}, \quad L_n = \begin{Bmatrix} L_{1,n} \\ L_{2,n} \\ L_{3,n} \\ L_{4,n} \end{Bmatrix}, \quad L_m = \begin{Bmatrix} L_{1,m} \\ L_{2,m} \\ L_{3,m} \\ L_{4,m} \end{Bmatrix}$$

where L_f is the friction-induced BLD, L_n is the BLD induced by axial deformation, and L_m is the BLD induced by bending deformation. The axial force is equal to the bearing friction:

$$n = f, \tag{5}$$

where f is the vector of the bearing friction (Fig. 9a); n is the vector of the axial force (Fig. 9b). The relationship between L_n and n can be expressed as:

$$n = K_n L_n, \tag{6}$$

where K_n is the axial stiffness matrix, and the moment vector m generated by the eccentric load can be expressed as:

$$m = \frac{H}{2} f, \tag{7}$$

where H is the section height (Fig. 9a).

The angular displacement of the section is calculated using Eq. (8):

$$\frac{H}{2} f = K_m \phi_m, \tag{8}$$

where K_m is the bending stiffness matrix.

L_m can be expressed using Eq. (9) based on the plane cross section assumption:

$$L_m = \frac{H}{2} \phi_m. \tag{9}$$

Substituting Eq. (9) into Eq. (8):

$$f = \frac{4}{H^2} K_m L_m. \tag{10}$$

Substituting Eq. (6) and Eq. (10) into Eq. (4) gives the equation for the friction-induced BLD:

$$L_f = \left(K_n^{-1} + \frac{H^2}{4} K_m^{-1} \right) f. \tag{11}$$

The friction-induced BLD of the fixed joint is restrained (such as the value of L_4 should be zero in Fig. 9); therefore, Eq. (11) is modified as:

$$L_f - L_4 = \left(K_n^{-1} + \frac{H^2}{4} K_m^{-1} \right) f. \tag{12}$$

While the maximum NBF switches into maximum PBF, $\Delta f = 2f$ and $\Delta L_f = 2L_f - 2L_4$. Equation (13) is reasonable:

$$\Delta L_f = (\Delta_n + \Delta_m) \Delta f, \tag{13}$$

where $\Delta_n = K_n^{-1}$, and $\Delta_m = K_m^{-1} H^2/4$.

The hysteresis parameter ΔL_f can reflect the multi-span girder bearing friction (i.e., bearing working performance), which is twice the friction-induced displacement in essence.

3.3 Evaluation index and assessment method

The BLD (y) is composed of the temperature-induced BLD (y_0) and friction-induced BLD (L_f); however, they are unobservable values except for the BLD. Generally, y_0 can be calculated based on the bridge temperature field. The BLD monitoring data can be divided into two parts, as shown in Fig. 8: BLD data in the maximum PBF state (y_P) and BLD data in the maximum NBF state (y_N). The hysteresis parameter (ΔL_f) can be obtained using Eq. (14):

$$\begin{cases} L_{f,P} = y_P - y_0 \\ L_{f,N} = y_N - y_0 \\ \Delta L_f = L_{f,P} - L_{f,N} \end{cases}. \tag{14}$$

From Eq. (13), an increase in the bearing friction (i.e., bearing degradation) causes ΔL_f to change proportionally. The evaluation index namely Ei is defined in Eq. (15), which can reflect the variation in the bearing friction. Figure 10 shows the flowchart of the methodology:

$$Ei = \|\Delta L_{f,d} - \Delta L_{f,h}\|_1, \tag{15}$$

where $\Delta L_{f,d}$ is the parameter after the degradation in the bearing working performance, and $\Delta L_{f,h}$ is the initial parameter.

An accurate calculation formula for y_0 is key to identifying the parameter. However, the temperature gradient significantly affects the BLD [15, 18], the linear regression algorithm may introduce significant errors when estimating y_0 , and machine learning algorithms have come across overfitting and underfitting. Therefore, the calculation formula for y_0 will be discussed in further detail based on a mechanical model.

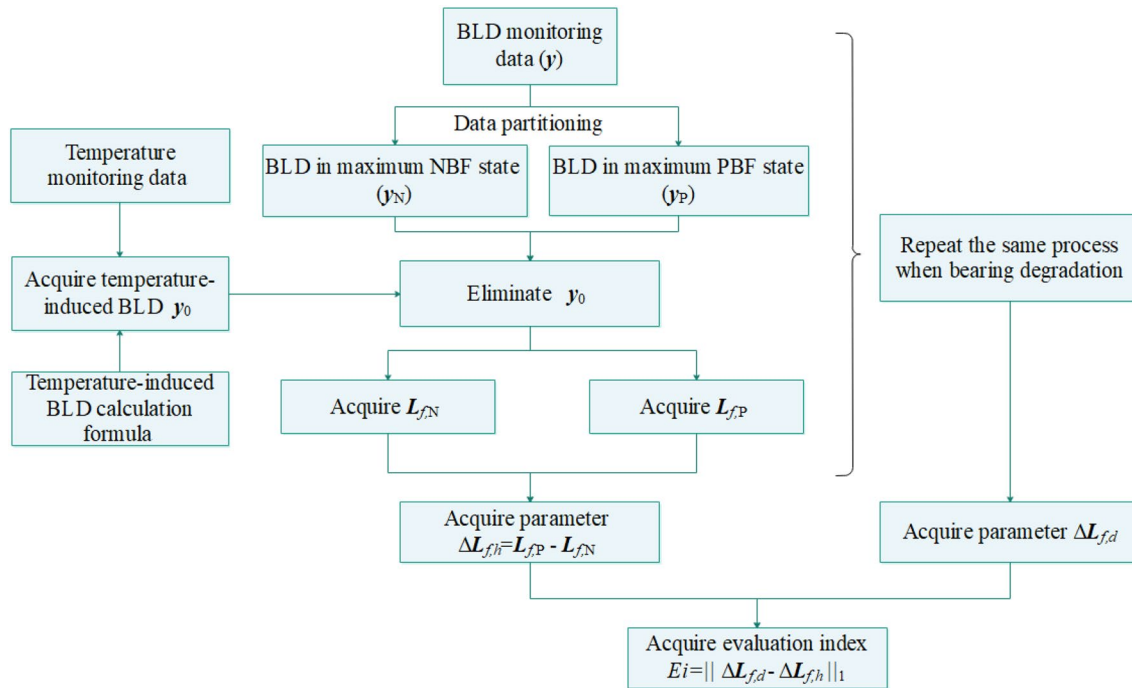


Fig. 10 Flowchart of the methodology

4 Calculation of temperature-induced BLD

Assumption

1. The mechanical behavior of the steel truss bridge meets the linear elasticity theory.
2. The temperature difference can describe the temperature gradient among the lower chord, the web member, and the upper chord.
3. The temperature-induced BLD is approximately equal to the axial deformation of the lower chord.
4. The hinged mode is used to simulate the connection of the truss members [25, 26] (Fig. 11).

Nomenclature for BLD calculation

- α : coefficient of thermal expansion, 10.0–12.0 $\mu\epsilon/^\circ\text{C}$.
- h_i : height of i th truss segment.
- l_i : length of i th truss segment.
- m_i : length of diagonal web member of i th truss segment.
- T : temperature of the lower chord.
- t : temperature difference between the lower and upper chords.
- T_m : temperature difference between the lower chord and the web member.
- E : modulus of elasticity of steel.
- A_i : cross-sectional area of the lower chord of the i th truss segment.

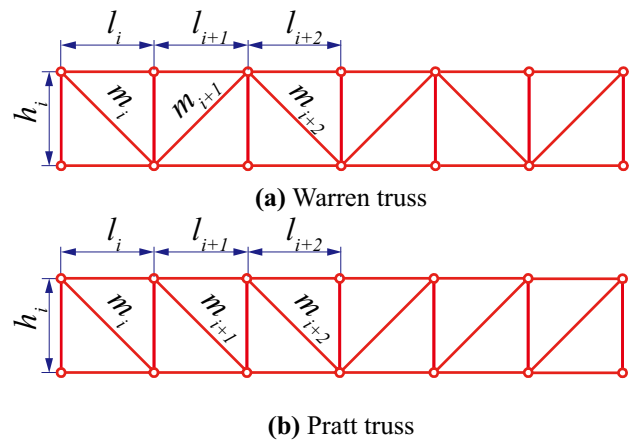


Fig. 11 Common form of parallel chord truss: a Warren truss; b Pratt truss

4.1 Calculation of BLD induced by T and t

While the lower chord temperature (T) and the temperature difference between the lower chord and the upper chord (t) load on the truss, the temperature gradient is equivalent to two parts (Fig. 12). Part 1 temperature gradient induces axial deformation, and Part 2 temperature gradient induces bending deformation.

First, the highly indeterminate structure is converted to the primary structure by releasing redundant restraint.

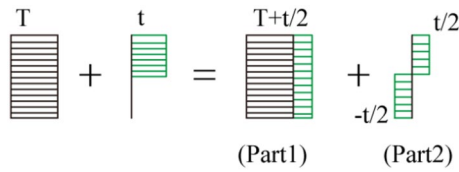


Fig. 12 Illustration of temperature gradient equivalence

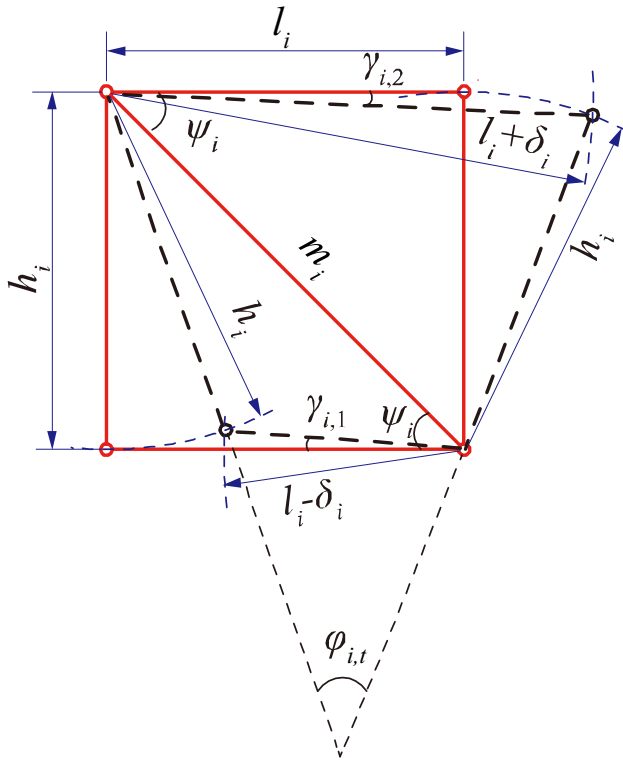


Fig. 13 The *i*th truss segment displacement due to Part 2 temperature gradient

Part 1:

The central axial deformation of the *i*th truss segment is obtained by:

$$L_{i,center,T,t} = \left(1 + \alpha T + \frac{\alpha t}{2}\right)l_i, \tag{16}$$

where $L_{i,center,T,t}$ is the center axial deformation of the *i*th truss segment induced by T and t .

Part 2:

The angular displacement of the *i*th truss segment vertical member results in the truss bending globally, and the displacement calculation of the *i*th truss segment is

illustrated in Fig. 13. The axial chord deformation of the *i*th truss segment is:

$$\delta_i = \frac{\alpha t l_i}{2}. \tag{17}$$

The length magnification of the chords λ is defined as:

$$\lambda = \frac{l_i \pm \delta_i}{l_i} = 1 \pm \frac{\alpha t}{2}, \tag{18}$$

where “+” is used for calculating the upper chord and “-” for the lower chord.

According to the law of cosines:

$$\begin{cases} \cos(\psi_i - \gamma_i) = \frac{m_i^2 + \lambda^2 l_i^2 - h_i^2}{2\lambda m_i l_i} \\ l_i^2 + h_i^2 = m_i^2 \end{cases}, \tag{19}$$

$$\cos(\psi_i - \gamma_i) = \left(\lambda + \frac{1}{\lambda}\right) \frac{l_i}{2m_i} = \frac{1}{2} \left(\lambda + \frac{1}{\lambda}\right) \cos\psi_i, \tag{20}$$

where ψ_i is the initial angle between the chord and the diagonal web member of the *i*th truss segment; γ_i is the angular displacement of the chord of the *i*th truss segment; more specifically from Fig. 13, $\gamma_{i,1}$ is the angular displacement of the lower chord, and $\gamma_{i,2}$ is the angular displacement of the upper chord. Considering αt is infinitesimal:

$$\cos(\psi_i - \gamma_{i,1}) - \cos(\psi_i - \gamma_{i,2}) = \frac{1}{2} \left(\alpha t - \frac{4\alpha t}{4 - \alpha^2 t^2}\right) \cos\psi_i \approx 0. \tag{21}$$

There is:

$$\cos(\psi_i - \gamma_{i,1}) \approx \cos(\psi_i - \gamma_{i,2}). \tag{22}$$

By monotonicity and continuity of the trigonometric function, the conclusion can be drawn:

$$\gamma_{i,1} \approx \gamma_{i,2}. \tag{23}$$

As a result, the chords are approximately parallel. Thus, we have:

$$\begin{cases} \varphi_{i,t} = \frac{2\delta_i}{h_i} \\ \rho_i = \frac{\varphi_{i,t}}{l_i} = \frac{\alpha t}{h_i} \end{cases}, \tag{24}$$

where $\varphi_{i,t}$ is the angular displacement of the vertical members of the *i*th truss segment, and ρ_i is the curvature of the *i*th truss segment. The proportional relationship between the center axial deformation and the chord axial deformation is:

$$\frac{L_{i,lower,T,t}}{L_{i,center,T,t}} = \frac{\frac{1}{\rho} - \frac{h_i}{2}}{\frac{1}{\rho}}, \tag{25}$$

where $L_{i,lower,T,t}$ is the lower chord deformation induced by T and t . Utilizing Eq. (16) and Eq. (25), $L_{i,lower,T,t}$ can be obtained by:

$$L_{i,lower,T,t} = \left(1 + \alpha T + \frac{\alpha t}{2}\right) \left(1 - \frac{\alpha t}{2}\right) l_i. \tag{26}$$

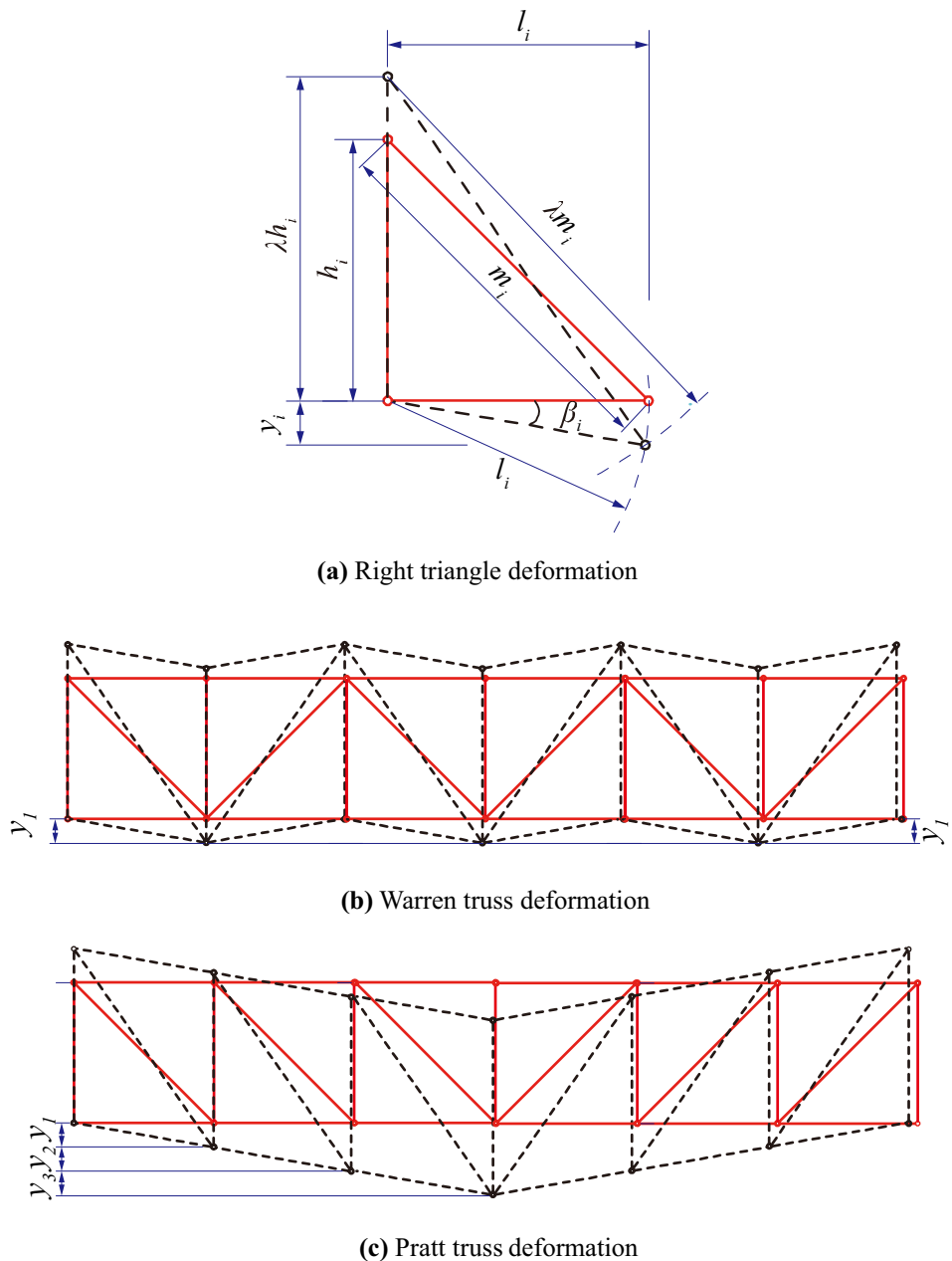
Second, while the vertical boundary conditions are considered, the effect of part 2 temperature gradient (Fig. 12)

is equal to the bending moment $M_{i,t}$ loading on the i th truss segment, which induces a constraint reaction of the indeterminate structure. The lower chord deformation induced by the constraint reaction is expressed by:

$$L_{i,lower,R,t} = \frac{N_{i,lower,R,t}}{EA_i} \propto R_t \propto M_{i,t} \propto t, \tag{27}$$

where R_t is the constraint reaction vector of the highly indeterminate structure induced by $M_{i,t}$; $L_{i,lower,R,t}$ is the lower chord axial deformation induced by R_t ; $N_{i,lower,R,t}$ is the lower chord axial force induced by R_t .

Fig. 14 Truss girder vertical displacement due to T_m : **a** right triangle deformation; **b** Warren truss deformation; **c** Pratt truss deformation



4.2 Calculation of BLD induced by T_m

The right triangle can describe the truss displacement induced by T_m (Fig. 14a). Given that the temperature of the web member changes, the Warren truss has a small vertical displacement globally (Fig. 14b); nevertheless, the Pratt truss exhibits displacement accumulation in the vertical direction (Fig. 14c).

The length of the web members becomes λ times due to T_m :

$$\lambda = 1 + \alpha T_m.$$

According to the cosine law:

$$\begin{cases} \cos\left(\beta_i + \frac{\pi}{2}\right) = \frac{l_i^2 + \lambda^2 h_i^2 - \lambda^2 m_i^2}{2\lambda l_i h_i} \\ l_i^2 + h_i^2 = m_i^2 \end{cases}, \tag{29}$$

where β_i is the angle displacement of the lower chord, expressed by:

$$\sin\beta_i = \left(\lambda - \frac{1}{\lambda}\right) \frac{l_i}{2h_i}. \tag{30}$$

The vertical displacement y_i is given by:

$$y_i = l_i \sin\beta_i = \left(\lambda - \frac{1}{\lambda}\right) \frac{l_i^2}{2h_i} = \frac{2\alpha T_m + \alpha^2 T_m^2}{1 + \alpha T_m} \frac{l_i^2}{2h_i}. \tag{31}$$

Because αT_m is infinitesimal, $\alpha^2 T_m^2$ is omitted as the higher-order terms:

$$y_i = \frac{l_i^2}{h_i} \frac{\alpha T_m}{1 + \alpha T_m}. \tag{32}$$

From Fig. 14c, the vertical displacement cumulant of the Pratt truss can be expressed by:

$$Y_n = \sum_{i=1}^n y_i, \tag{33}$$

where n is the number of truss segments. While the boundary conditions are introduced, the constraint reaction is given by:

$$F_{T_m} = KY = \frac{l_i^2}{h_i} \frac{\alpha T_m}{1 + \alpha T_m} Kx, \tag{34}$$

where F_{T_m} is the vector of the constraint reaction; K is the stiffness matrix of structure; Y is the vector of the vertical displacement at constraint position; x is the position vector of the constraint. The proportional relationship can be obtained by:

$$L_{i,lower,R,T_m} = \frac{N_{i,lower,R,T_m}}{EA_i} \propto \frac{F_{T_m}}{EA_i} \propto \frac{l_i^2}{EA_i h_i} \frac{\alpha T_m}{1 + \alpha T_m} Kx, \tag{35}$$

where $L_{i,lower,R,T_m}$ is the lower chord deformation induced by T_m ; $N_{i,lower,R,T_m}$ is the lower chord axial force induced by F_{T_m} .

The temperature-induced BLD comprises three parts:

$$L_{lower,T,t,T_m} = \sum_{i=1}^n L_{i,lower,T,t} + \sum_{i=1}^n L_{i,lower,R,t} + \sum_{i=1}^n L_{i,lower,R,T_m}. \tag{36}$$

A concise form is proposed:

$$L_{lower,T,t,T_m} = \alpha L[1 + Q(t)]T + R(t) + S(T_m), \tag{37}$$

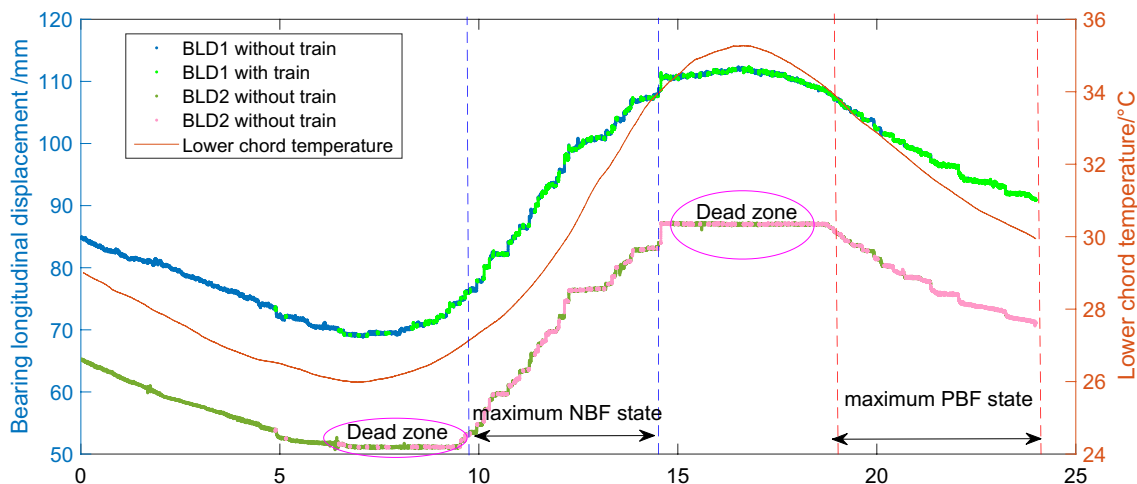
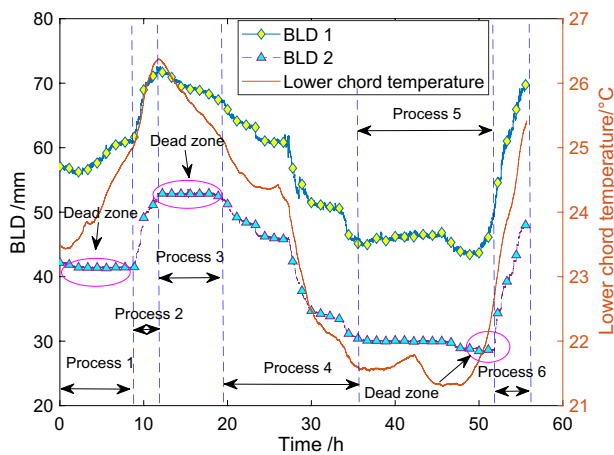
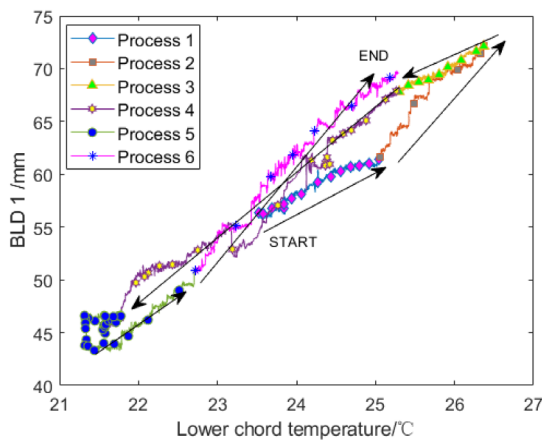


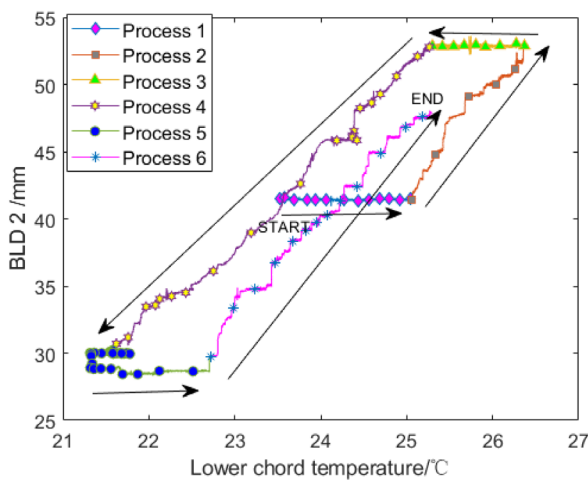
Fig. 15 Time history of BLD 1 and BLD 2



(a) time history of BLD1 and BLD 2 and temperature



(b) BLD 1 and temperature



(c) BLD 2 and temperature

Fig. 16 The BLD and temperature relationship: **a** time history of BLD 1 and BLD 2 and temperature; **b** BLD 1 and temperature; **c** BLD 2 and temperature

where L is the original length of the lower chord; $Q(t)$, $R(t)$, and $S(T_m)$ are functions of an independent variable. Compared with the Pratt truss, the Warren truss can ignore the effect induced by T_m because of the little accumulation of the vertical displacement.

5 Field validation and application

Figure 15 shows the BLD 1~2 data sequence of the truss bridge shown in Fig. 1. As shown, the trend in each BLD is synchronous and similar. Comparing Fig. 8 with Fig. 15, bearing 2 has significant hysteretic frictional characteristics, yet bearing 1 does not.

The friction direction of bearing 3 is switched frequently because of train passing (Fig. 6), so it is indescribable to bearing 3 friction. The friction effect of bearing 3 is treated as noise, while BLD 1 and BLD 2 are studied. Equation (38) is the equivalent of Eq. (13):

$$\begin{Bmatrix} \Delta L_{f,1} \\ \Delta L_{f,2} \end{Bmatrix} = \Delta_{mn} \begin{Bmatrix} \Delta f_1 \\ \Delta f_2 \end{Bmatrix}, \tag{38}$$

where Δf_i is twice the maximum static friction in Eq. (38), and $\Delta L_{f,i}$ is the hysteresis parameter, where the subscript i represents the bearing number. $\Delta_{mn} \in \mathbb{R}^{2 \times 2}$. About three cloudy days of continuous monitoring data are employed to validate hysteretic frictional characteristics when the truss temperature gradient is weak and stable, and the lower chord temperature (the mean of G1 and G2 shown in Figs. 1 and 2) is proportional to the temperature-induced BLD. From Fig. 16a, the entire process can be divided into six processes.

For BLD 1:

- Process 1: Maximum NBF state.
- Process 2: Maximum NBF state.
- Process 3: Maximum PBF state.
- Process 4: Maximum PBF state.
- Process 5: Maximum PBF state.
- Process 6: Maximum NBF state.

For BLD 2:

- Process 1: PBF state switches to NBF state,
- Process 2: Maximum NBF state,
- Process 3: Dead zone, NBF state switches to PBF state,
- Process 4: Maximum PBF state,
- Process 5: Dead zone, PBF state switches to NBF state,
- Process 6: Maximum NBF state,

In processes 2 and 3 of BLD 1 (Fig. 16b), a weak dead zone indicates $\Delta L_{f,1}$ may be negative or close to zero. Only BLD 2 represents a clear hysteresis loop (Fig. 16c).

While considering the temperature gradient, 20 sunny days of continuous monitoring data, including the temperature and BLD, were employed to assess the bearing working

Table 1 Temperature variable of monitor data

Variable	T	t	$T_m = t$
Values	$(G1 + G2)/2$	$(G1 + G2)/2 - (G3 + G4)/2$	$(G1 + G2)/2 - (G3 + G4)/2$

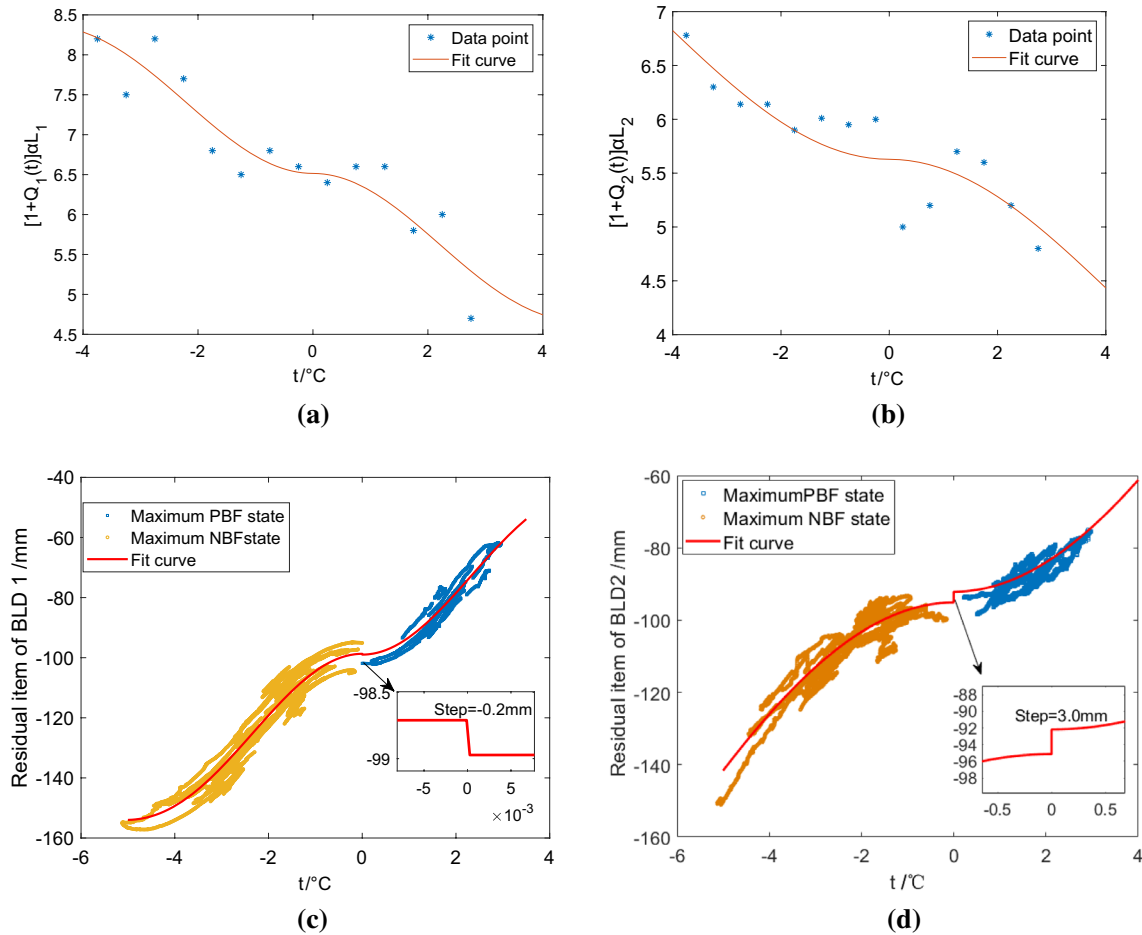


Fig. 17 Regression models based on temperature-induced BLD: **a** $[1 + Q_1(t)]\alpha L_1$ and t ; **b** $[1 + Q_2(t)]\alpha L_2$ and t ; **c** $R_1(t) + S_1(t) + B_1 \pm \Delta L_{f,1}/2$ and t ; **d** $R_2(t) + S_2(t) + B_2 \pm \Delta L_{f,2}/2$ and t

performance. The temperature of the web member was made approximately equal to the temperature of the upper chord given the approximately same solar radiation. The temperature variables are listed in Table 1, where G1–G4 correspond to the monitoring data of the temperature sensors (Fig. 2).

For the process shown in Fig. 10, the data of the maximum PBF state and maximum NBF state are selected from the monitoring data. We used a convenient method to calculate the parameters.

Controlling the change in t by $0.5\text{ }^\circ\text{C}$ at each stage, the linear characteristic of the partial correlation between BLD and T is solved to determine $[1 + Q_i(t)]\alpha L_i$. The $R_i(t) + S_i(t) + B_i \pm \Delta L_{f,i}/2$ named residual item can be obtained by Eq. (39):

$$\begin{cases} R_i(t) + S_i(t) + B_i + \frac{\Delta L_{f,i}}{2} = y_{P,i} - [1 + Q_i(t)]\alpha L_i T \\ R_i(t) + S_i(t) + B_i - \frac{\Delta L_{f,i}}{2} = y_{N,i} - [1 + Q_i(t)]\alpha L_i T \end{cases}, \quad i = 1, 2, \quad (39)$$

where $y_{P,i}$ is the BLD i in the maximum PBF state; $y_{N,i}$ is the BLD i in the maximum NBF state; B_i is the initial value of BLD i . The step value of the fitting curve is equal to the parameter $\Delta L_{f,i}$, where $\Delta L_{f,1} = -0.2\text{ mm}$ (Fig. 17c), $\Delta L_{f,2} = 3.0\text{ mm}$ (Fig. 17d). Figure 18 shows the error of the regression model. The parameter $\Delta L_{f,2}$ indicates that bearing 2 has a significant friction hysteresis. The parameters can be calculated in the same manner after bearing degradation (Fig. 10). Based on the evaluation index (Ei) obtained from

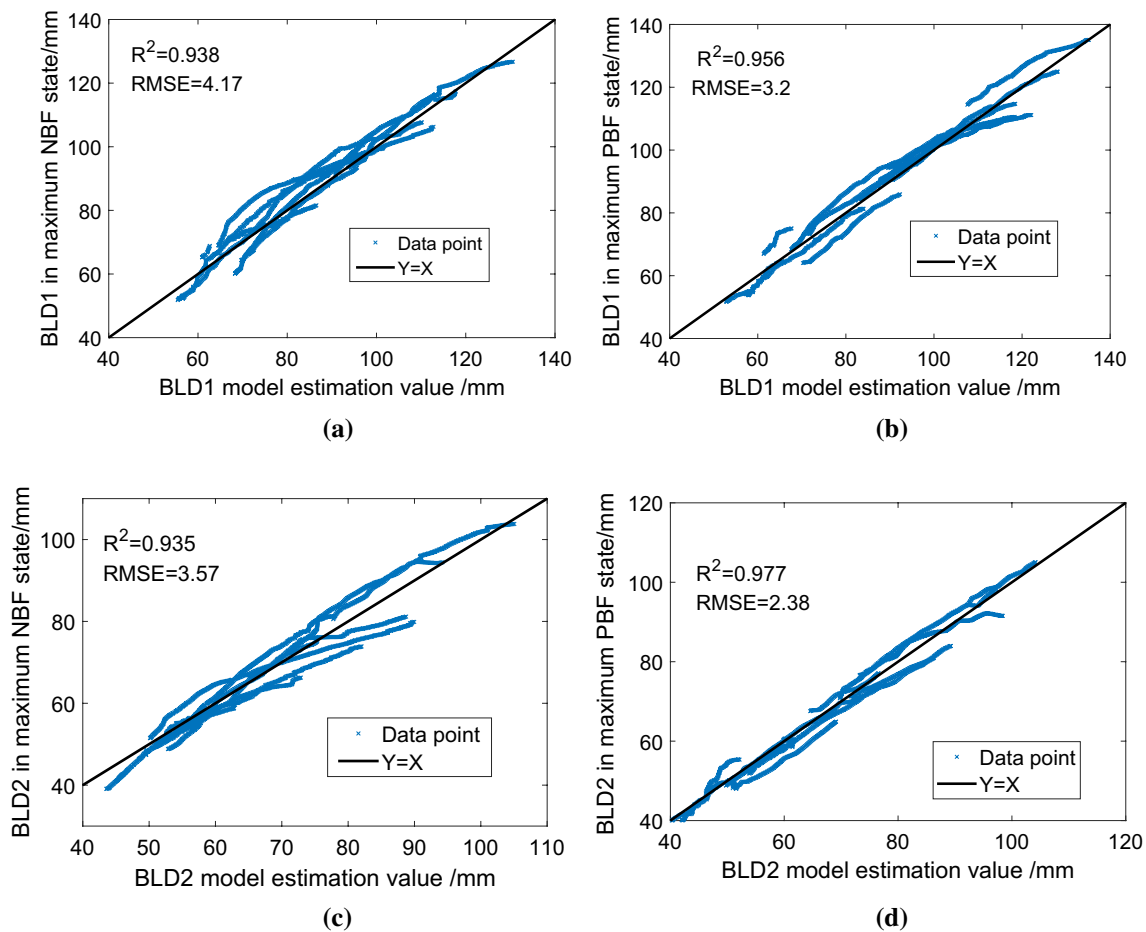


Fig. 18 Error analysis of regression model: **a** BLD 1 in maximum NBF state; **b** BLD 1 in maximum PBF state; **c** BLD 2 in maximum NBF state; **d** BLD 2 in maximum PBF state

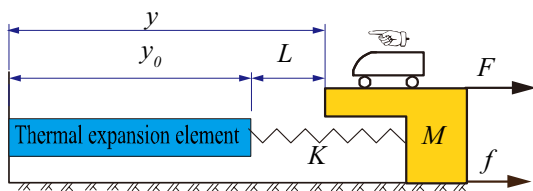


Fig. 19 The model of BLD on the effect of the temperature and friction and train longitudinal force

Eq. (15), the variation in the maximum bearing friction can be identified. The evaluation index is proportional to the bearing friction. Further, the bearing friction can be obtained from the parameters when the structural stiffness is known.

6 Conclusions and discussions

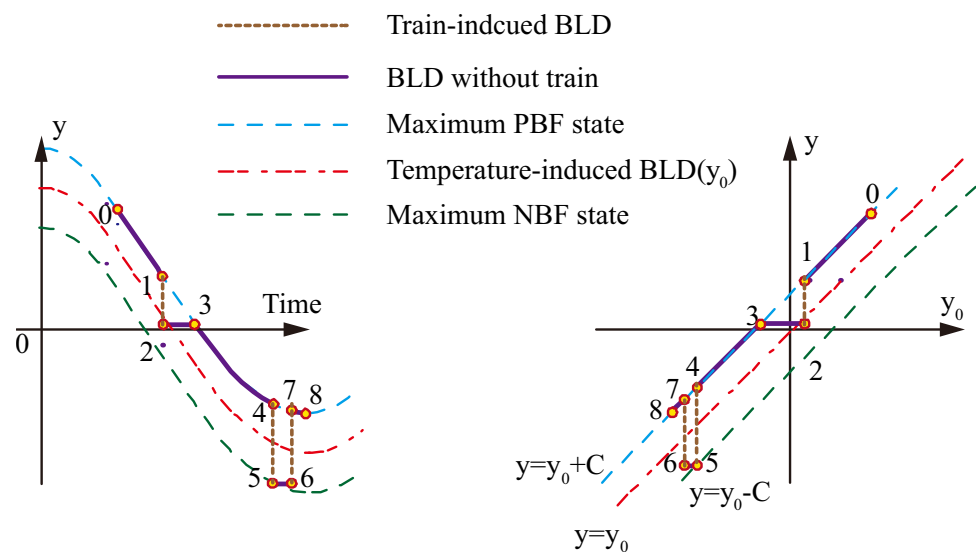
This paper proposed an assessment method for the performance of multispan continuous truss bridge bearings. The evaluation index of the BLD based on a friction hysteresis model could

reflect the variation in the bearing friction, thus realizing the evaluation of the bearing performance. When a beam is subjected to periodic temperature loads with sufficient fluctuation, the continuous maximum NBF state and maximum NBF state data sequence could be observed. Based on the short-term monitoring data of the actual truss arch bridge considering the temperature gradient, the temperature-induced BLD calculation formula deduced in this study was verified. It is recommended to use the evaluation index to reflect the degradation in the bearing performance based on long-term monitoring data.

However, the following three aspects require further studies:

1. BLD 1 is affected by the bearing friction; however, it does not reflect the evident friction hysteresis characteristics like BLD 2 in Fig. 16. The effect of bearing 2 friction may counteract the effect of bearing 1 friction on BLD 1 because the bearing friction is eccentric, which needs to be verified.
2. In fact, the supporting pier or rubber bearing as a flexible body may produce significant horizontal deformation

Fig. 20 The influence of train longitudinal force on BLD



when subjected to bearing friction. Theoretically, a flexible body can be treated as a spring connected in series at the end of the beam [18]; however, the feasibility of the method requires more in-depth research in this case.

3. The train longitudinal force may break the BLD motion path of the friction hysteresis model. The analysis model is proposed in Fig. 19:

In Fig. 19, F represents the train longitudinal force, which is opposite to the train driving direction. While the train runs over the bridge, the beam undergoes spring force, bearing friction (f), and train longitudinal force (F) in the longitudinal direction. The train longitudinal force may change BLD (y); this can in turn change the bearing friction. Figure 20 represents the effect of the train briefly. Path 1–2, path 4–5, and path 6–7 are induced by train, and path 2–3, path 5–6 fall into the dead zone. While the train-induced BLD, such as path 1–2, path 4–5, and path 6–7 in Fig. 20, occurs frequently, the path friction hysteresis model of BLD is broken by train longitudinal force, and the maximum NBF state and maximum PBF state of the bearing cannot be captured easily. Consequently, the continuous maximum NBF state and the maximum NBF state data sequence are indistinct in the time domain. In this case, it is impossible to establish a relationship between the temperature, BLD, and maximum bearing friction without the longitudinal force of the train; therefore, the friction hysteresis model cannot be used to evaluate the bearing working performance. Considering the impact of trains, the evaluation of the bearing needs further research.

Acknowledgements This work was supported by the National Key Research and Development Project, China (Grant nos. 2016YFB1200401-107), Key Research and Development Project of

Hebei Province, China (Grant nos.19210804D), Shijiazhuang Tiedao University State Key Laboratory of Mechanical Behavior and System Safety of Traffic Engineering Structures (Grant nos. ZZ2020-19).

References

1. Lima JM, de Brito J (2009) Inspection survey of 150 expansion joints in road bridges. *Eng Struct* 31(5):1077–1084
2. Roeder CW (1998) Fatigue and dynamic load measurements on modular expansion joints. *Constr Build Mater* 12(2):143–150
3. Sun Z, Zhang Y (2016) Failure mechanism of expansion joints in a suspension bridge. *J Bridge Eng (ASCE)* 21(10):05016005
4. Okuda M, Yumiyama S, Ikeda H (2004) Reinforcement of expansion joint on Akashi Kaikyo Bridge. In: JSCE 59th Annual Meeting, Japan Society of Civil Engineers
5. Tong Guo MASCE, Liu J et al (2015) Displacement monitoring and analysis of expansion joints of long-span steel bridges with viscous dampers. *Bridge Eng* 20:04014099
6. Xia Q, Xia Y, Wan H et al (2020) Condition analysis of expansion joints of a long-span suspension bridge through metamodel-based model updating considering thermal effect. *Struct Control Health Monit* 27:e2521
7. Xia Y, Chen B, Zhou XQ, Xu Y-L (2013) Field monitoring and numerical analysis of Tsing Ma Suspension Bridge temperature behavior. *Struct Control Health Monit* 20:560–575
8. Charles RF, David AJ (1998) Comparative study of damage identification algorithms applied to a bridge: II. Numerical study. *Smart Mater Struct* 7:720
9. Zhou LM, Zhang J, Xu F (2021) Efficient flexibility identification method using structured target rank approximation and extended prony's method. *J Sound Vib* 4:116254
10. Han Q, Ma Q, Xu J et al (2021) Structural health monitoring research under varying temperature condition: a review. *J Civ Struct Health Monit* 11(3):1–25
11. Ni YQ, Hua XG, Wong KY et al (2007) Assessment of bridge expansion joints using long-term displacement and temperature measurement. *J Perform Constr Facil (ASCE)* 21(2):143–151
12. Yang D, Aiqun L, Youliang D (2009) Research and application of correlation between beam end displacement and temperature

- of long-span suspension bridge. *J Highw Transp Res Dev* 26(5):54–58
13. Ni YQ, Wang YW, Zhang C (2020) A Bayesian approach for condition assessment and damage alarm of bridge expansion joints using long-term structural health monitoring data. *Eng Struct* 212:110520
 14. Huang HB, Yi TH, Li HN, Liu H (2018) New representative temperature for performance alarming of bridge expansion joints through temperature–displacement relation-ship. *J Bridge Eng (ASCE)* 23(7):04018043
 15. Wang GX, Ding YL, Song YS et al (2016) Detection and location of the degraded bearings based on monitoring the longitudinal expansion performance of the main girder of the Dasheng-guan Yangtze Bridge. *J Perform Constr Facil* 30(4):383–384
 16. Yarnold MT, Moon FL (2015) Temperature-based structural health monitoring baseline for long-span bridges. *Eng Struct* 86:157
 17. Winkler J, Specialist C, Hansen DH (2018) Innovative long-term monitoring of the great belt bridge expansion joint using digital image correlation. *Struct Eng Int* 28(3):347–352
 18. Yarnold MT, Moon FL, Aktan AE (2015) Temperature-based structural identification of long-span bridges. *J Struct Eng* 141:04015027
 19. Murphy B, Yarnold M (2018) Temperature-driven structural identification of a steel girder bridge with an integral abutment. *Eng Struct* 155:209
 20. Xia Q, Zhou L, Zhang J (2018) Thermal performance analysis of a long-span suspension bridge with long-term monitoring data. *J Civ Struct Health Monit* 8(4):543–553
 21. Zhou S, Song W (2018) Environmental effects embedded model updating method considering environmental impacts. *Struct Control Health Monit* 25:e2116
 22. Jesus A, Brommer P, Zhu YJ, Laory I (2017) Comprehensive Bayesian structural identification using temperature variation. *Eng Struct* 141:75–82
 23. Jesus A, Brommer P, Westgate R, Koo K, Brownjohn JMW, Laory I (2019) Bayesian structural identification of a long suspension bridge considering temperature and traffic load effects. *Struct Health Monit* 18(4):1310–1323
 24. Alexander J, Yarnold M (2020) Quasi-static bearing evaluation and monitoring—a case study. *Front Built Environ* 6:69
 25. Dengguo T, Zongliang Ai (2009) Study about effect of nodal stiffness of continuous steel truss girder bridge on internal forces in structure. *Railw Eng* 9:1–3 (**in Chinese**)
 26. Qiang G, Tianli H, Long C et al (2019) Influence of stiffness of integral joints on mechanical properties of steel truss girder bridges. *J Civ Eng Manag* 36(5):144–156 (**in Chinese**)

Publisher's Note Springer Nature remains neutral with regard to jurisdictional claims in published maps and institutional affiliations.